Integrated analysis reveals the protective mechanism and therapeutic potential of hyperbaric oxygen against pulmonary fibrosis

Yuan Yuan[1#], Guoqiang Qiao[1#], Jiajiao Zhou[1], Yilu Zhou[2,3], Yali Li[1], Xia Li[1*], Zhenglin Jiang[1*], Yihua Wang[2,3*]

[1]Department of Neurophysiology and Neuropharmacology, Institute of Special Environmental Medicine and Co-innovation Center of Neuroregeneration, Nantong University, Nantong, Jiangsu Province, 226019, PR China;
[2]Biological Sciences, Faculty of Environmental and Life Sciences, University of Southampton, Southampton, SO17 1BJ, United Kingdom;
[3]Institute for Life Sciences, University of Southampton, Southampton, SO17 1BJ, United Kingdom.

[#]These authors contributed equally and share the first authorship.

*Correspondence: Yihua Wang (yihua.wang@soton.ac.uk); Zhenglin Jiang (jiangzl@ntu.edu.cn) or Xia Li (lixia7979@ntu.edu.cn).

Abstract

Idiopathic pulmonary fibrosis (IPF) is a dreadful, chronic, and irreversibly progressive disease leading to death with few effective treatments. Our previous study suggested that repetitive hyperbaric oxygen (HBO) treatment alleviates bleomycin-induced pulmonary fibrosis in mice. Here, we investigated the protective mechanism of HBO treatment against pulmonary fibrosis using an integrated approach. Analyzing publicly available expression data from the mouse model of bleomycin-induced pulmonary fibrosis as well as IPF patients, several potential mechanisms of relevance to IPF pathology were identified, including increased epithelial-to-mesenchymal transition (EMT) and glycolysis. High EMT or glycolysis scores in bronchoalveolar lavage (BAL) were strong independent predictors of mortality in multivariate analysis. These processes were potentially driven by hypoxia and blocked by HBO treatment. Together, these data support HBO treatment as a viable strategy against pulmonary fibrosis.

Keywords: epithelial-mesenchymal transition, hyperbaric oxygen, hypoxia, pulmonary fibrosis, systematic analysis.

Introduction

Idiopathic pulmonary fibrosis (IPF) is a chronic, progressive and fatal interstitial lung disease, characterized by excessive deposition of extracellular matrix (ECM) in the lung parenchyma, leading to the destroyed alveolar architecture and disrupted lung functions. It has a poor prognosis and limited treatment options.[1] Recently, pulmonary fibrosis is reported to be a long-term outcome associated with major morbidity after COVID-19 infection,[2-4] therefore, draws increasing attention. Novel and effective approaches to treat pulmonary fibrosis are urgently needed.

Previously we reported that hyperbaric oxygen (HBO) treatment attenuates a single dose of intratracheal administrated bleomycin-induced pulmonary fibrosis in mice,[5] however, the underlying molecular mechanism is to be clarified. HBO treatment is to inhale pure oxygen under a pressure of more than 1 atmosphere absolute (ATA). It significantly increases the dissolved oxygen in plasma and the diffusion distance of oxygen, therefore, is applied in clinics for the treatment of a variety of diseases with underlying hypoxia.[6] Here we sought to investigate the protective mechanism of HBO treatment against pulmonary fibrosis using an integrated approach.

Materials and methods

Integrative analysis

The flow charts of data collection from the bleomycin-induced mouse model (microarray) and IPF patients (RNA-seq) are provided in Fig. S1, with a summary of datasets in Supplementary Tables S1-S3. A detailed description of data merging analysis, including uniform manifold approximation and projection (UMAP) analysis, differential expression genes (DEGs) analysis, gene ontology (GO) enrichment, and gene set enrichment analysis (GSEA), is provided in the Supplementary Methods.

Animal experiments

Animals used in this study were purchased from the Experimental Animal Center of Nantong University (Institutional License: SYXK(SU)-2012-0030). Mice were maintained in the individually ventilated cages (IVC), under a 12-hour light/12-hour dark cycle, and were allowed to eat and drink *ad libitum* throughout the study. Animal experiments in this study were approved by the Animal Ethics Committee at Nantong University (Approval No: S20200315-005), and all the experiments conformed to the relevant regulatory standards. The bleomycin-induced pulmonary fibrosis mouse model was constructed and treated with HBO as previously reported.[5] The hematoxylin and eosin (H/E) staining was performed to confirm the presence of pulmonary fibrosis. The details of these experiments can be found in the Supplementary Methods.

RNA-seq and bioinformatic analysis

RNA isolation and mRNA sequencing of lung tissues were performed following the manufacturer's instructions. Paired-end strategy (2×150) on the Illumina NovaSeq 6000 platform was adopted. The quality control of raw reads, mapping, identification of DEGs, as well as GO term enrichment analysis and GSEA were performed with details provided in the Supplementary Methods. The RNA-seq data have been deposited in the Gene Expression Omnibus (GEO) database (accession code GSE200109).

Gene set variation analysis (GSVA) score calculation

To assess the activity of a specific pathway, GSVA package[7] (version 1.40.1) was used to calculate the score. The Hallmark gene sets of epithelial-mesenchymal transition (EMT) and glycolysis were used to calculate EMT and glycolysis scores, respectively. A 15-gene expression signature (*ACOT7*, *ADM*, *ALDOA*, *CDKN3*, *ENO1*, *LDHA*, *MIF*, *MRPS17*, *NDRG1*, *P4HA1*, *PGAM1*, *SLC2A1*, *TPI1*, *TUBB6*, and *VEGFA*), which enables classification of hypoxia-inducible factor (HIF) activity,[8, 9] was used to calculate the HIF score.

Hazard ratio and survival analysis

To assess the hazard ratio (HR), EMT score and glycolysis score were used to construct the univariate Cox proportional hazards model through survminer (version 0.4.9) in RStudio. The log-rank tests were used to compare Kaplan-Meier survival curves between each group by the survival package (v3.2-3). EMT score, glycolysis score, and GAP (gender, age, physiological) score, which is provided in GSE70867,[10] were used to construct the multivariate Cox proportional hazard model via the survminer (version 0.4.9) in RStudio. The log-rank and Cox $P < 0.05$ were considered statistically significant.

Real-time qPCR analysis

Genes of interest were detected by RT-qPCR using SYBR green as the indicator. The details of the experimental process, as well as primers, are provided in the Supplementary Methods.

Western blot analysis

Protein samples from mice lung tissues were lysed with RIPA buffer (Beyotime Biotechnology, China) containing protease inhibitor (Meilunbio, Liaoning, China). Primary antibodies targeting E-cadherin (Cat#3195, Cell Signaling Technology, USA) and β-actin (Cat#A5316, Sigma-Aldrich, USA) were used. Signals were detected using

an ECL detection system with Tanon 5200 Multi imaging system (Shanghai, China), and evaluated by ImageJ 1.42q software (National Institutes of Health).

Lactate measurement

The lactate levels in the lung tissues were detected by the L-lactic acid/lactate (LA) colorimetric assay kit (Cat#E-BC-K044-M, Elabscience Biotechnology, China) following the manufacturer's instructions.

Statistical analysis

Statistical analyses were performed in GraphPad Prism (version 9.0). Data are presented as mean and standard deviation (s.d.). The choice of analytical method depends on whether the data follow a normal distribution and variance homogeneity. The comparison between the two groups was performed using either two-sample *t*-test or Mann-Whitney *U* test. A false discovery rate calculated through the two-stage step-up method of the Benjamini, Krieger and Yekutieli method was adopted in the multiple comparisons. One-way ANOVA or Kruskal-Wallis test was used to compare more than two groups of data. The Dunnett test was used for multiple comparisons. We evaluated the correlations between the EMT score, Glycolysis score and HIF score using Pearson's correlation. Results were considered significant as $P < 0.05$ or false discovery rate (FDR) $Q < 0.05$.

Code availability

Codes were implemented in R and have been deposited in GitHub:
https://github.com/claw60/IPF

Data availability

All data supporting the findings of the current study are listed in the Supplementary Materials.

Results

Integrative analysis reveals the activation of EMT and glycolysis in pulmonary fibrosis.

A total of 213 murine lung samples were collected from 10 Gene Expression Omnibus (GEO) datasets (Fig. S1A), including 90 control lungs and 123 bleomycin-challenged lungs collected at different time points (Tables S1 and S2). After batch effects removal by cross-platform normalization, 2 clear clusters corresponding to control and bleomycin-challenged lungs, respectively, were visualized using Uniform Manifold Approximation and Projection (UMAP) analysis (Fig. S2). A total of 6,914 genes, which were present in all the samples, were included in the following analysis. In addition, 6 GEO datasets of human lung samples were collected, including 167 control lungs from healthy donors and 205 IPF lungs (Fig. S1B; Table S3). Following batch effects removal, samples were classified into control and IPF groups (Fig. S3). DEGs were identified followed by further analysis (Fig. S4; Tables S4-S11). Details of the protocol were provided in the Supplementary Methods.

GO enrichment analysis identified several IPF-related pathological terms, including extracellular matrix and collagen (Tables S12-S19). GSEA based on the 50 well-characterized hallmark gene sets from the Molecular Signature Database (MSigDB)[11] identified the activation of EMT and glycolysis in bleomycin-challenged mice lungs at different time points, in IPF lungs as well as bronchoalveolar lavage (BAL) samples from IPF patients[10] (Fig. 1A).

The activation of EMT in bleomycin-challenged mice lungs (Fig. S5) was verified by checking the expression levels of several EMT markers, including *Cdh1* (encoding E-cadherin, an epithelial marker), *Vim* (encoding vimentin, a mesenchymal marker), *Mmp2* (encoding matrix metallopeptidase 2), *Acta2* (encoding α-smooth muscle actin, α-SMA, a myofibroblast marker), *Fn1* (encoding fibronectin) and *Col1a1* (encoding type I collagen). We observed a decrease in the level of *Cdh1* and an increase in the levels of *Vim*, *Mmp2*, *Acta2*, *Fn1*, and *Col1a1* in bleomycin-challenged mice lungs at day 7 or day 21 post instillation (Fig. 1B and C). These results confirmed activation of EMT in the development of pulmonary fibrosis induced by bleomycin in mice.

EMT and glycolysis scores in BAL predict mortality in IPF patients.

We next investigated whether EMT and glycolysis scores had prognostic values in the BAL cohort. IPF patients were classified into score-high or score-low groups based on an optimal cutoff value automatically determined by the algorithm. We identified that both the EMT score and glycolysis score were able to predict survival in the IPF cohort (Fig. 2A and B; hazard ratio, HR: 23 and $P = 1.41 \times 10^{-8}$ for the EMT score; HR: 19 and $P = 8.71 \times 10^{-6}$ for the glycolysis score). Multivariate analysis suggested that a high EMT score or a high glycolysis score was a strong independent predictor of mortality including in multivariate analysis with the physiological Gender, Age, and Physiology (GAP) score that uses commonly measured clinical and physiologic variables to predict mortality in IPF[12] (Fig. 2C; HR: 12.4 and $P < 0.001$ for the EMT score; HR: 5.1, $P = 0.036$ for the glycolysis score).

EMT and glycolysis activation during pulmonary fibrosis is potentially driven by hypoxia.

Hypoxia is known to activate EMT and glycolysis.[13-16] In consistence with a recent report,[17] the HIF score, an indicator of hypoxia-inducible factor (HIF) activity calculated using a 15 gene signature,[8, 9] was significantly increased in IPF lungs (Fig. 3A) as well as BAL samples (Fig. 3B) from IPF patients. In addition, the HIF score was elevated in bleomycin-challenged mice lungs from day 2 to day 21 post instillation (Fig. 3C). The induction of HIF activity in bleomycin-challenged mice lungs (Fig. S5) was further verified by checking the expression levels of these 15 genes,[8, 9] including *ACOT7*, *ADM*, *ALDOA*, *CDKN3*, *ENO1*, *LDHA*, *MIF*, *MRPS17*, *NDRG1*, *P4HA1*, *PGAM1*, *SLC2A1*, *TPI1*, *TUBB6*, and *VEGFA*, in mice lungs at day 7 and day 21 post bleomycin treatment.

Among the 15 genes, *PGAM1*, *TPI1*, *MIF*, *ALDOA*, *LDHA*, *ENO1*, *VEGFA*, and *P4HA1* are also included in the Hallmark glycolysis gene set, therefore can partially represent the glycolysis status as well. On day 7 post bleomycin treatment, the expression levels of *Adm*, *Aldoa*, *Cdkn3*, *Eno1*, *Ndrg1*, *Pgam1*, *Slc2a1*, *Tpi1*, and *Tubb6* were all elevated (all $Q < 0.05$). There was a trend of increase in the expression level of *Acot7* and *Mif*, although statistical significance wasn't reached ($Q = 0.06$ and $Q = 0.09$, respectively). On day 21 post bleomycin treatment, the expression levels of *Adm*, *Aldoa*,

Cdkn3, *Eno1*, *Mif*, *Mrps17*, *Slc2a1*, and *Tpi1* were all significantly upregulated (all $Q < 0.01$) (Fig. 3D and E). Together, these results demonstrated that HIF activity is induced in mice lungs upon bleomycin challenge.

We then investigated whether EMT and glycolysis activation occurs during the development of pulmonary fibrosis in the context of hypoxia. The HIF score correlated strongly with an EMT signature in IPF lungs (Fig. 3F; $R = 0.47$, $P = 2.6 \times 10^{-16}$), BAL samples (Fig. 3G; $R = 0.42$, $P = 6.3 \times 10^{-10}$) and bleomycin-challenged mice lungs (Fig. 3H; $R = 0.56$, $P = 2.3 \times 10^{-16}$). These correlations were also observed between the HIF score and glycolysis score (Fig. 3I-K).

The protective mechanism of HBO against pulmonary fibrosis.

We previously reported that repetitive HBO treatment started from day 7 post bleomycin instillation significantly alleviates lung fibrosis in mice (Fig. 4A and B).[5] To determine the underlying molecular mechanism, we characterized the global transcriptomic changes in bleomycin-challenged mice lungs exposed to HBO by performing RNA-Seq. Genes with a *P* value less than 0.05 and fold change above 1.5 were considered as differentially expressed genes (DEGs). In total, 1,221 DEGs were identified, including 651 upregulated and 570 downregulated genes (Fig. 4C; Table S20). GO enrichment analysis identified "extracellular matrix" as the top enriched term in down-regulated genes for the cellular component classification, consistent with our previous findings[18] (Fig. 4D; Table S21). GSEA identified several pathways inhibited upon HBO treatment in bleomycin-challenged mice lungs, including the above identified EMT, glycolysis, and hypoxia (Fig. 4E). The findings were further confirmed by GSVA showing decreases in HIF, EMT, and glycolysis scores upon HBO exposure in bleomycin-challenged mice lungs (Fig. 5A-C).

The effects of HBO on the HIF activity in the lungs from mice challenged with bleomycin were verified by checking several HIF target genes, including *Adm*, *Cdkn3*, *Eno1*, *Pgam1*, *Slc2a1*, and *Tubb6*. All their expressions were decreased upon HBO exposure in bleomycin-challenged mice lungs (Fig. 5D; all *Q* values < 0.05, except for *Mif* with $Q = 0.06$). EMT induction in bleomycin-challenged mice lungs was also blocked by HBO exposure, at least partially, reflected by an increase in mRNA expression of *Cdh1* (E-cadherin, $Q = 0.07$), and a significant reduction in *Vim*, *Acta2*,

232 *Fn1*, *and Col1a1* (Fig. 5E; all *Q* values < 0.05). The effect of HBO on E-cadherin was
233 further confirmed using western blots showing that its protein level was increased upon
234 HBO treatment in the lungs of the bleomycin-challenged mice (Fig. 5F; $P < 0.05$). In
235 addition, we observed an elevated lactate level (a marker of glycolytic shift) in the lungs
236 of the bleomycin-challenged mice, and this was reduced upon HBO treatment (Fig. 5G).
237 Together these data supported the roles of HBO treatment in inhibiting EMT and
238 glycolysis.

Discussion

In this study, several potential mechanisms of relevance to pulmonary fibrosis were identified, including increased EMT and glycolysis, which are strong independent predictors of mortality in IPF patients. These processes are potentially driven by hypoxia and blocked by HBO treatment.

The role of EMT in pulmonary fibrosis has been proposed previously.[19-21] Recent studies suggest that instead of contributing to the extracellular matrix producing fibroblast population directly, alveolar epithelial type II (ATII) cells undergoing EMT promotes a pro-fibrotic microenvironment through paracrine signalings, which enhances TGF-β-induced fibroblast activation.[22-26] Glycolytic reprogramming is found to be active in IPF patients,[27, 28] and promotes myofibroblast differentiation,[29] a key event in pulmonary fibrosis formation. Glycolysis inhibition is proven to alleviate pulmonary fibrosis in bleomycin-induced mouse model.[30-32] Hypoxia is known to drive EMT and glycolytic shift,[29, 33-35] and HIF is required for these processes.[29, 33, 34] As a hallmark feature of pulmonary fibrosis,[36, 37] hypoxia signaling pathway has been found active in IPF patients,[38-46] while HIF is upregulated in lung tissues from both IPF patients and the bleomycin-induced pulmonary fibrosis mouse model.[17, 39, 41, 44, 47] Consistent with these reports, the HIF score was significantly increased in bleomycin-challenged mice lungs, IPF lungs as well as BAL samples from IPF patients, and its increase correlated with an upregulated EMT and glycolysis signature.

Since HBO increases the partial pressure of oxygen, the soluble oxygen in plasma, and the diffuse distance of oxygen,[48] it has been shown to counter tissue hypoxia with high efficacy. HBO alleviates hypoxia in multiple conditions, including the hypoxemia caused by COVID-19 infection,[49] solid tumors,[50-52] and focal cerebral ischemia model.[53] In our previous study, we provided evidence that HBO treatment reduces HIF-1α levels in lung fibroblast induced by TGF-β,[5] supports the role of HBO in reversing hypoxia. It was reported that HBO ameliorates the EMT phenomenon in keloid tissue,[54] induces mesenchymal-to-epithelial transition in a dimethyl-alpha-benzantracene mammary rat adenocarcinoma model revealed by gene expression profiling,[55] and represses EMT and Warburg effect in hypoxic NSCLC cells.[56] Further perturbation experiments are needed to demonstrate that the HBO treatment relies on glycolysis and/or EMT to prevent lung fibrosis.

Together with these reports, our study helps to provide a unified concept for the protective mechanism of HBO against pulmonary fibrosis: HBO alleviates hypoxia during the development of pulmonary fibrosis, so inhibiting IPF-related pathological processes such as EMT and glycolysis. Given the general safety of HBO in the long-term clinical practice,[57-59] these data suggest a realistic scenario of a prospective clinical trial in IPF patients with HBO treatment.

Author contributions

Yuan Yuan: Conceptualization, Methodology, Investigation, Project administration, Writing-Original Draft preparation, Funding acquisition; **Qiao Guoqiang**: Formal analysis, Investigation, Methodology, Validation, Writing-Original draft preparation; **Zhou Jiajiao**: Data curation, Validation; **Zhou Yilu:** Methodology, Software; **Li Yali:** Methodology; **Li Xia:** Supervision, Funding acquisition; **Jiang Zhenglin:** Supervision, Funding acquisition, Writing-Reviewing, and Editing; **Wang Yihua**: Conceptualization, Methodology, Supervision, Funding acquisition, Writing-Reviewing, and Editing.

Conflict of Interests

The authors declare that they have no competing interests.

Acknowledgements

YY was supported by Natural Science Research of Jiangsu Higher Education Institutions of China (19KJB320002), the Science and Technology Project of Nantong City (JC2020010), and a Research Startup Fund of Nantong University. YW was supported by the UK Medical Research Council (MR/S025480/1) and the UK Royal Society (IEC\NSFC\191030). ZJ was supported by the National Natural Science Foundation of China (82171869, 81671859). XL was supported by the Science and Technology Project of Nantong City (MS12020019, JC2021079). For the purpose of open access, the authors have applied a CC-BY public copyright license to any Author Accepted Manuscript version arising from this submission.

References

1. Richeldi L, Collard HR, Jones MG. Idiopathic pulmonary fibrosis. *Lancet*. May 13 2017;389(10082):1941-1952. doi:10.1016/S0140-6736(17)30866-8

2. Mylvaganam RJ, Bailey JI, Sznajder JI, Sala MA, Northwestern Comprehensive CCC. Recovering from a pandemic: pulmonary fibrosis after SARS-CoV-2 infection. *Eur Respir Rev*. Dec 31 2021;30(162)doi:10.1183/16000617.0194-2021

3. Zhang C, Wu Z, Li JW, et al. Discharge may not be the end of treatment: Pay attention to pulmonary fibrosis caused by severe COVID-19. *J Med Virol*. Mar 2021;93(3):1378-1386. doi:10.1002/jmv.26634

4. Wu X, Liu X, Zhou Y, et al. 3-month, 6-month, 9-month, and 12-month respiratory outcomes in patients following COVID-19-related hospitalisation: a prospective study. *Lancet Respir Med*. Jul 2021;9(7):747-754. doi:10.1016/S2213-2600(21)00174-0

5. Yuan Y, Li Y, Qiao G, et al. Hyperbaric Oxygen Ameliorates Bleomycin-Induced Pulmonary Fibrosis in Mice. *Front Mol Biosci*. 2021;8:675437. doi:10.3389/fmolb.2021.675437

6. Ortega MA, Fraile-Martinez O, Garcia-Montero C, et al. A General Overview on the Hyperbaric Oxygen Therapy: Applications, Mechanisms and Translational Opportunities. *Medicina (Kaunas)*. Aug 24 2021;57(9)doi:10.3390/medicina57090864

7. Hanzelmann S, Castelo R, Guinney J. GSVA: gene set variation analysis for microarray and RNA-seq data. *BMC Bioinformatics*. Jan 16 2013;14:7. doi:10.1186/1471-2105-14-7

8. Buffa FM, Harris AL, West CM, Miller CJ. Large meta-analysis of multiple cancers reveals a common, compact and highly prognostic hypoxia metagene. *Br J Cancer*. Jan 19 2010;102(2):428-35. doi:10.1038/sj.bjc.6605450

9. Ye Y, Hu Q, Chen H, et al. Characterization of hypoxia-associated molecular features to aid hypoxia-targeted therapy. *Nature Metabolism*. 2019/04/01 2019;1(4):431-444. doi:10.1038/s42255-019-0045-8

10. Prasse A, Binder H, Schupp JC, et al. BAL Cell Gene Expression Is Indicative of Outcome and Airway Basal Cell Involvement in Idiopathic Pulmonary Fibrosis. *Am J Respir Crit Care Med*. Mar 1 2019;199(5):622-630. doi:10.1164/rccm.201712-2551OC

11. Liberzon A, Birger C, Thorvaldsdottir H, Ghandi M, Mesirov JP, Tamayo P. The Molecular Signatures Database (MSigDB) hallmark gene set collection. *Cell Syst*. Dec 23 2015;1(6):417-425. doi:10.1016/j.cels.2015.12.004

12. Ley B, Ryerson CJ, Vittinghoff E, et al. A multidimensional index and staging system for idiopathic pulmonary fibrosis. *Ann Intern Med*. May 15 2012;156(10):684-91. doi:10.7326/0003-4819-156-10-201205150-00004

13. Hapke RY, Haake SM. Hypoxia-induced epithelial to mesenchymal transition in cancer. *Cancer Lett*. Sep 1 2020;487:10-20. doi:10.1016/j.canlet.2020.05.012

14. Tam SY, Wu VWC, Law HKW. Hypoxia-Induced Epithelial-Mesenchymal Transition in Cancers: HIF-1alpha and Beyond. *Front Oncol*. 2020;10:486. doi:10.3389/fonc.2020.00486

15. Denko NC. Hypoxia, HIF1 and glucose metabolism in the solid tumour. *Nat Rev Cancer*. Sep 2008;8(9):705-13. doi:10.1038/nrc2468

16. Kierans SJ, Taylor CT. Regulation of glycolysis by the hypoxia-inducible factor (HIF): implications for cellular physiology. *J Physiol*. Jan 2021;599(1):23-37. doi:10.1113/JP280572

17. Zhou Y, Ewing RM, Davies DE, Wang Y, Jones MG. A validated hypoxia-inducible factor (HIF) signature across tissue compartments predicts clinical outcome in human lung fibrosis. *medRxiv*. 2022-01-01 00:00:00 2022;

18. Yuan Y, Zhou Y, Li Y, et al. Deconvolution of RNA-Seq Analysis of Hyperbaric Oxygen-Treated Mice Lungs Reveals Mesenchymal Cell Subtype Changes. *Int J Mol Sci*. Feb 18 2020;21(4):1371. doi:10.3390/ijms21041371

19. Sakuma Y. Epithelial-to-mesenchymal transition and its role in EGFR-mutant lung adenocarcinoma and idiopathic pulmonary fibrosis. *Pathol Int*. Aug 2017;67(8):379-388. doi:10.1111/pin.12553

20. Salton F, Volpe MC, Confalonieri M. Epithelial(-)Mesenchymal Transition in the Pathogenesis of Idiopathic Pulmonary Fibrosis. *Medicina (Kaunas)*. Mar 28 2019;55(4):83. doi:10.3390/medicina55040083

21. Phan THG, Paliogiannis P, Nasrallah GK, et al. Emerging cellular and molecular determinants of idiopathic pulmonary fibrosis. *Cell Mol Life Sci*. Mar 2021;78(5):2031-2057. doi:10.1007/s00018-020-03693-7

22. Yao L, Conforti F, Hill C, et al. Paracrine signalling during ZEB1-mediated epithelial-mesenchymal transition augments local myofibroblast differentiation in lung fibrosis. *Cell Death Differ*. May 2019;26(5):943-957. doi:10.1038/s41418-018-0175-7

23. Hill C, Jones MG, Davies DE, Wang Y. Epithelial-mesenchymal transition contributes to pulmonary fibrosis via aberrant epithelial/fibroblastic cross-talk. *J Lung Health Dis*. Apr 2 2019;3(2):31-35.

24. Yao L, Zhou Y, Li J, et al. Bidirectional epithelial-mesenchymal crosstalk provides self-sustaining profibrotic signals in pulmonary fibrosis. *J Biol Chem*. Sep 2021;297(3):101096. doi:10.1016/j.jbc.2021.101096

25. Zhou Y, Hill C, Yao L, et al. Quantitative Proteomic Analysis in Alveolar Type II Cells Reveals the Different Capacities of RAS and TGF-beta to Induce Epithelial-Mesenchymal Transition. *Front Mol Biosci*. 2021;8:595712. doi:10.3389/fmolb.2021.595712

26. Hill C, Li J, Liu D, et al. Autophagy inhibition-mediated epithelial-mesenchymal transition augments local myofibroblast differentiation in pulmonary fibrosis. *Cell Death Dis*. Aug 7 2019;10(8):591. doi:10.1038/s41419-019-1820-x

27. Maher TM. Aerobic Glycolysis and the Warburg Effect. An Unexplored Realm in the Search for Fibrosis Therapies? *Am J Respir Crit Care Med*. Dec 15 2015;192(12):1407-9. doi:10.1164/rccm.201508-1699ED

28. Chen Z, Liu M, Li L, Chen L. Involvement of the Warburg effect in non-tumor diseases processes. *J Cell Physiol*. Apr 2018;233(4):2839-2849. doi:10.1002/jcp.25998

29. Goodwin J, Choi H, Hsieh MH, et al. Targeting Hypoxia-Inducible Factor-1alpha/Pyruvate Dehydrogenase Kinase 1 Axis by Dichloroacetate Suppresses Bleomycin-induced Pulmonary Fibrosis. *Am J Respir Cell Mol Biol*. Feb 2018;58(2):216-231. doi:10.1165/rcmb.2016-0186OC

30. Xie N, Tan Z, Banerjee S, et al. Glycolytic Reprogramming in Myofibroblast Differentiation and Lung Fibrosis. *Am J Respir Crit Care Med*. Dec 15 2015;192(12):1462-74. doi:10.1164/rccm.201504-0780OC

31. Chen W, Zhang J, Zhong W, et al. Anlotinib Inhibits PFKFB3-Driven Glycolysis in Myofibroblasts to Reverse Pulmonary Fibrosis. *Front Pharmacol*. 2021;12:744826. doi:10.3389/fphar.2021.744826

32. Wang Z, Chen L, Huang Y, et al. Pharmaceutical targeting of succinate dehydrogenase in fibroblasts controls bleomycin-induced lung fibrosis. *Redox Biol*. Oct 2021;46:102082. doi:10.1016/j.redox.2021.102082

33. Delbrel E, Uzunhan Y, Soumare A, et al. ER Stress is Involved in Epithelial-To-Mesenchymal Transition of Alveolar Epithelial Cells Exposed to a Hypoxic Microenvironment. *Int J Mol Sci*. Mar 14 2019;20(6):1299. doi:10.3390/ijms20061299

34. Zhou G, Dada LA, Wu M, et al. Hypoxia-induced alveolar epithelial-mesenchymal transition requires mitochondrial ROS and hypoxia-inducible factor 1. *Am J Physiol Lung Cell Mol Physiol*. Dec 2009;297(6):L1120-30. doi:10.1152/ajplung.00007.2009

35. Guo L, Xu JM, Liu L, Liu SM, Zhu R. Hypoxia-Induced Epithelial-Mesenchymal Transition Is Involved in Bleomycin-Induced Lung Fibrosis. *Biomed Res Int*. 2015;2015:232791. doi:10.1155/2015/232791

36. Lokmic Z, Musyoka J, Hewitson TD, Darby IA. Hypoxia and hypoxia signaling in tissue repair and

fibrosis. *Int Rev Cell Mol Biol*. 2012;296:139-85. doi:10.1016/B978-0-12-394307-1.00003-5

37. Plantier L, Cazes A, Dinh-Xuan AT, Bancal C, Marchand-Adam S, Crestani B. Physiology of the lung in idiopathic pulmonary fibrosis. *Eur Respir Rev*. Mar 31 2018;27(147)doi:10.1183/16000617.0062-2017

38. Yamazaki R, Kasuya Y, Fujita T, et al. Antifibrotic effects of cyclosporine A on TGF-beta1-treated lung fibroblasts and lungs from bleomycin-treated mice: role of hypoxia-inducible factor-1alpha. *Faseb J*. Aug 2017;31(8):3359-3371. doi:10.1096/fj.201601357R

39. Tzouvelekis A, Harokopos V, Paparountas T, et al. Comparative expression profiling in pulmonary fibrosis suggests a role of hypoxia-inducible factor-1alpha in disease pathogenesis. *Am J Respir Crit Care Med*. Dec 1 2007;176(11):1108-19. doi:10.1164/rccm.200705-683OC

40. Qian F, He M, Duan W, et al. Cross regulation between hypoxia-inducible transcription factor-1α (HIF-1α) and transforming growth factor (TGF)-β1 mediates nickel oxide nanoparticles (NiONPs)-induced pulmonary fibrosis. *Am J Transl Res*. 2015;7(11):2364-78.

41. Aquino-Galvez A, Gonzalez-Avila G, Jimenez-Sanchez LL, et al. Dysregulated expression of hypoxia-inducible factors augments myofibroblasts differentiation in idiopathic pulmonary fibrosis. *Respir Res*. Jun 24 2019;20(1):130. doi:10.1186/s12931-019-1100-4

42. Xie H, Tan JT, Wang RL, Meng XX, Tang X, Gao S. Expression and significance of HIF-1alpha in pulmonary fibrosis induced by paraquat. *Exp Biol Med (Maywood)*. Sep 2013;238(9):1062-8. doi:10.1177/1535370213498978

43. Philip K, Mills TW, Davies J, et al. HIF1A up-regulates the ADORA2B receptor on alternatively activated macrophages and contributes to pulmonary fibrosis. *Faseb J*. Nov 2017;31(11):4745-4758. doi:10.1096/fj.201700219R

44. Ueno M, Maeno T, Nomura M, et al. Hypoxia-inducible factor-1alpha mediates TGF-beta-induced PAI-1 production in alveolar macrophages in pulmonary fibrosis. *Am J Physiol Lung Cell Mol Physiol*. May 2011;300(5):L740-52. doi:10.1152/ajplung.00146.2010

45. Kusko RL, Brothers JF, 2nd, Tedrow J, et al. Integrated Genomics Reveals Convergent Transcriptomic Networks Underlying Chronic Obstructive Pulmonary Disease and Idiopathic Pulmonary Fibrosis. *Am J Respir Crit Care Med*. Oct 15 2016;194(8):948-960. doi:10.1164/rccm.201510-2026OC

46. Burman A, Kropski JA, Calvi CL, et al. Localized hypoxia links ER stress to lung fibrosis through induction of C/EBP homologous protein. *JCI Insight*. Aug 23 2018;3(16):e99543. doi:10.1172/jci.insight.99543

47. Brereton CJ, Yao L, Davies ER, et al. Pseudohypoxic HIF pathway activation dysregulates collagen structure-function in human lung fibrosis. *Elife*. Feb 21 2022;11doi:10.7554/eLife.69348

48. Choudhury R. Hypoxia and hyperbaric oxygen therapy: a review. *Int J Gen Med*. 2018;11:431-442. doi:10.2147/IJGM.S172460

49. Paganini M, Bosco G, Perozzo FAG, et al. The Role of Hyperbaric Oxygen Treatment for COVID-19: A Review. *Adv Exp Med Biol*. 2021;1289:27-35. doi:10.1007/5584_2020_568

50. Kinoshita Y, Kohshi K, Kunugita N, Tosaki T, Yokota A. Preservation of tumour oxygen after hyperbaric oxygenation monitored by magnetic resonance imaging. *Br J Cancer*. Jan 2000;82(1):88-92. doi:10.1054/bjoc.1999.0882

51. Beppu T, Kamada K, Yoshida Y, Arai H, Ogasawara K, Ogawa A. Change of oxygen pressure in glioblastoma tissue under various conditions. *J Neurooncol*. May 2002;58(1):47-52. doi:10.1023/a:1015832726054

52. Thews O, Vaupel P. Temporal changes in tumor oxygenation and perfusion upon normo- and hyperbaric inspiratory hyperoxia. *Strahlenther Onkol*. Mar 2016;192(3):174-81. doi:10.1007/s00066-015-0916-1

53. Sun L, Marti HH, Veltkamp R. Hyperbaric oxygen reduces tissue hypoxia and hypoxia-inducible factor-1 alpha expression in focal cerebral ischemia. *Stroke*. Mar 2008;39(3):1000-6.

441 doi:10.1161/STROKEAHA.107.490599

442 54. Zhang M, Liu S, Guan E, et al. Hyperbaric oxygen therapy can ameliorate the EMT phenomenon
443 in keloid tissue. *Medicine (Baltimore)*. Jul 2018;97(29):e11529. doi:10.1097/MD.0000000000011529

444 55. Moen I, Oyan AM, Kalland KH, et al. Hyperoxic treatment induces mesenchymal-to-epithelial
445 transition in a rat adenocarcinoma model. *PLoS One*. Jul 28 2009;4(7):e6381.
446 doi:10.1371/journal.pone.0006381

447 56. Zhang L, Ke J, Min S, et al. Hyperbaric Oxygen Therapy Represses the Warburg Effect and
448 Epithelial-Mesenchymal Transition in Hypoxic NSCLC Cells via the HIF-1alpha/PFKP Axis. *Front*
449 *Oncol*. 2021;11:691762. doi:10.3389/fonc.2021.691762

450 57. Camporesi EM. Side effects of hyperbaric oxygen therapy. *Undersea Hyperb Med*. May-Jun
451 2014;41(3):253-7.

452 58. Hadanny A, Meir O, Bechor Y, Fishlev G, Bergan J, Efrati S. The safety of hyperbaric oxygen
453 treatment--retrospective analysis in 2,334 patients. *Undersea Hyperb Med*. Mar-Apr 2016;43(2):113-22.

454 59. Hadanny A, Zubari T, Tamir-Adler L, et al. Hyperbaric oxygen therapy effects on pulmonary
455 functions: a prospective cohort study. *BMC Pulm Med*. Aug 13 2019;19(1):148. doi:10.1186/s12890-
456 019-0893-8

457

Figure legends

Figure 1 Integrative analysis reveals the activation of EMT and glycolysis in pulmonary fibrosis. **(A)** Scatter plot showing GSEA from 6 categories (development, immune, metabolism, pathway, proliferation, and signaling). The sizes of circles represent the −Log10 of the adjusted *P* values and the colors of circles represent the normalized enrichment score (NES). **(B and C)** Fold change in the mRNA levels of EMT markers in the lungs from saline-treated (Control) or bleomycin-challenged mice (BLM) at day 7 **(B)** or day 21 **(C)** post instillation. *Actb* (β-actin) -normalized mRNA levels in the control group were used to set the baseline value at unity. Data are mean ± s.d..*Q < 0.05, **Q < 0.01, by two sample Mann-Whitney *U* test, multiple comparisons using false discovery rate (*Q*) with the method of two-stage step-up (Benjamini, Krieger and Yekutieli).

Figure 2 EMT and glycolysis scores in BAL predict mortality in IPF patients. **(A and B)** Kaplan-Meier plots show the overall survival in IPF patients with low *vs*. high EMT scores **(A)** or glycolysis scores **(B)** in BAL. *P* values, hazard ratio (HR), 95% confidence interval (CI), and patient number (n) are indicated. **(C)** Multivariate analysis in IPF patients. HR, 95% CI, patient number (n) and *P* values are shown.

Figure 3 EMT and glycolysis activation during pulmonary fibrosis is potentially driven by hypoxia. **(A and B)** Violin plots showing HIF scores in the lungs **(A)** and BAL samples **(B)** from healthy control *vs*. IPF patients. ***P <0.001, by two sample Mann-Whitney *U* test. **(C)** Violin plot showing HIF scores in the lungs from control or bleomycin-treated mice at multiple time points post instillation. **P <0.01, ***P <0.001, by Dunnett's multiple comparisons test. **(D and E)** Fold change in the mRNA levels of multiple HIF target genes in the lungs from saline-treated (Control) or bleomycin-challenged mice (BLM) at day 7 **(D)** or day 21 **(E)** post instillation. *Actb* (β-actin) -normalized mRNA levels in the control group were used to set the baseline value at unity. Data are mean ± s.d..*Q < 0.05, **Q < 0.01, by two sample Mann-Whitney *U* test, multiple comparisons using false discovery rate (*Q*) with the method of two-

stage step-up (Benjamini, Krieger and Yekutieli). **(F-H)** Scatter plots showing the correlation between the HIF score and EMT score in IPF lungs **(F)**, BAL samples, **(G)** and lungs from bleomycin-challenged mice **(H)**. **(I-K)** Scatter plots showing the correlation between HIF score and glycolysis score in IPF lungs **(I)**, BAL samples, **(J)** and lungs from bleomycin-challenged mice **(K)**. Pearson *R*-values and *P* values are indicated.

Figure 4 The protective mechanism of HBO against pulmonary fibrosis. **(A)** Schematic diagram of the experimental procedure (details in the Supplementary Methods). **(B)** Lung tissues from bleomycin-challenged mice (BLM) or bleomycin-challenged mice treated with repetitive HBO exposure (BLM + HBO) were stained with H/E. The left panel shows the whole section of the left lung lobe (scale bar: 1 mm) with higher magnification images of the box area in the corresponding right panel (scale bar: 100 μm). **(C-D)** Global transcriptomic changes are identified in bleomycin-challenged mice lungs exposed to HBO by performing RNA-Seq. **(C)** Volcano plot showing DEGs (P <0.05 and fold change > 1.5) analyzed by DEseq2. Up- and down-regulated genes are highlighted in red and blue, respectively. **(D)** Bar chart summarizing GO enrichment results analyzed by Metascape. Up- and down-regulated terms, as well as –log10 (P), are indicated. **(E)** Bubble chart showing the GSEA results. The sizes of circles represent the count of genes detected in the pathway and the colors of circles represent the −Log10 of the adjusted *P* values. NES represents the normalized enrichment score.

Figure 5 Effects of HBO treatment on hypoxia and EMT. **(A-C)** Graphs showing the HIF score **(D)**, EMT score **(E)** and glycolysis score **(F)** in the lungs from bleomycin-challenged mice (BLM) or bleomycin-challenged mice with repetitive HBO exposure (BLM + HBO). *P < 0.05, **P < 0.01, by two-sample *t*-test. **(D-E)** Fold change in the mRNA levels of multiple HIF target genes **(D)** and EMT markers **(E)** in the lungs from bleomycin-challenged mice (BLM) or bleomycin-challenged mice treated with repetitive HBO exposure (BLM + HBO) at 21d post bleomycin instillation. *Actb* (β-actin) -normalized mRNA levels in the BLM group were used to set the baseline value at unity. Data are mean ± s.d..*Q < 0.05, **Q < 0.01, by two-sample Mann-Whitney *U* test, multiple comparisons using false discovery rate (Q) with the method of two-stage step-up (Benjamini, Krieger and Yekutieli). **(F)** Protein expression of E-cadherin

in the lungs from bleomycin-challenged mice (BLM) or bleomycin-challenged mice treated with repetitive HBO exposure (BLM + HBO). β-actin was used as a loading control. β-actin-normalized protein levels in bleomycin-challenged mice lungs (BLM) were used to set the baseline value at unity. Data are mean ± s.d., n = 4 samples in each group. *$P < 0.05$, analyzed by two sample *t* test. **(G)** The lactate level in mice lungs with the indicated treatment. Data are mean ± s.d., n = 5 samples in each group. *$P < 0.05$, **$P < 0.01$, analyzed by one-way ANOVA test.

Figure 1

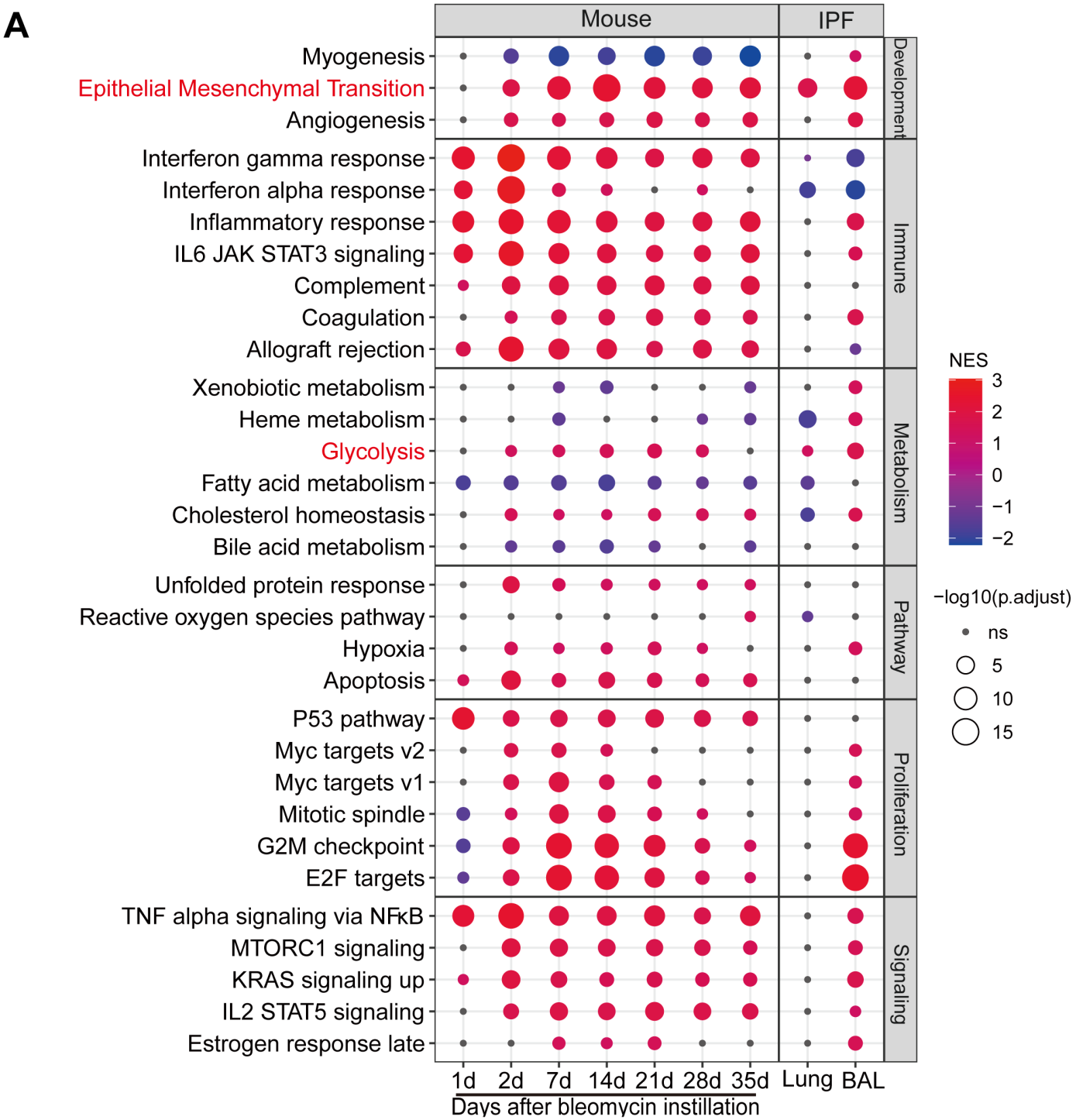
A
Mouse
IPF
Development
Immune
Metabolism
Pathway
Proliferation
Signaling
Myogenesis
Epithelial Mesenchymal Transition
Angiogenesis
Interferon gamma response
Interferon alpha response
Inflammatory response
IL6 JAK STAT3 signaling
Complement
Coagulation
Allograft rejection
Xenobiotic metabolism
Heme metabolism
Glycolysis
Fatty acid metabolism
Cholesterol homeostasis
Bile acid metabolism
Unfolded protein response
Reactive oxygen species pathway
Hypoxia
Apoptosis
P53 pathway
Myc targets v2
Myc targets v1
Mitotic spindle
G2M checkpoint
E2F targets
TNF alpha signaling via NFkB
MTORC1 signaling
KRAS signaling up
IL2 STAT5 signaling
Estrogen response late
1d 2d 7d 14d 21d 28d 35d Lung BAL
Days after bleomycin instillation
NES
3
2
1
0
−1
−2
−log10(p.adjust)
ns
5
10
15

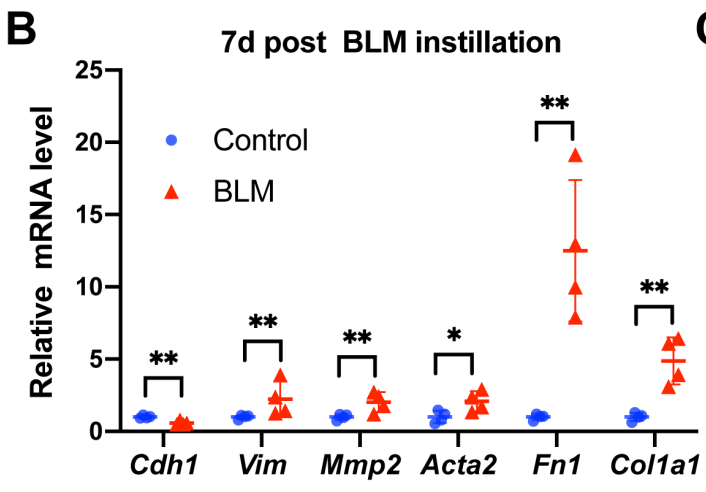
B
7d post BLM instillation
Relative mRNA level
Control
BLM
Cdh1
Vim
Mmp2
Acta2
Fn1
Col1a1

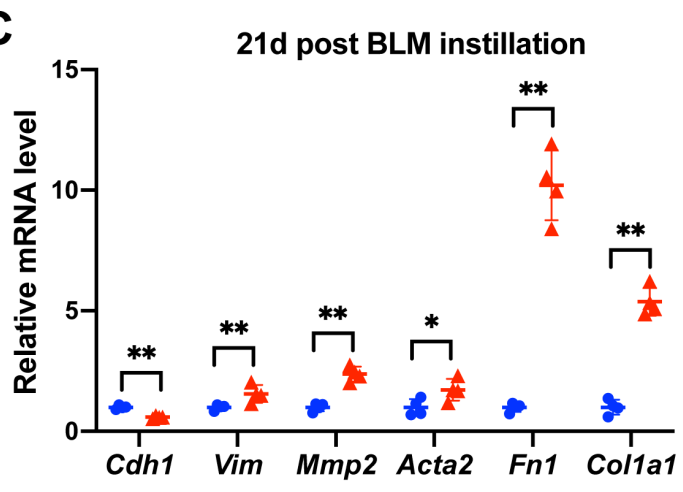
C
21d post BLM instillation
Relative mRNA level
Cdh1
Vim
Mmp2
Acta2
Fn1
Col1a1

Figure 2

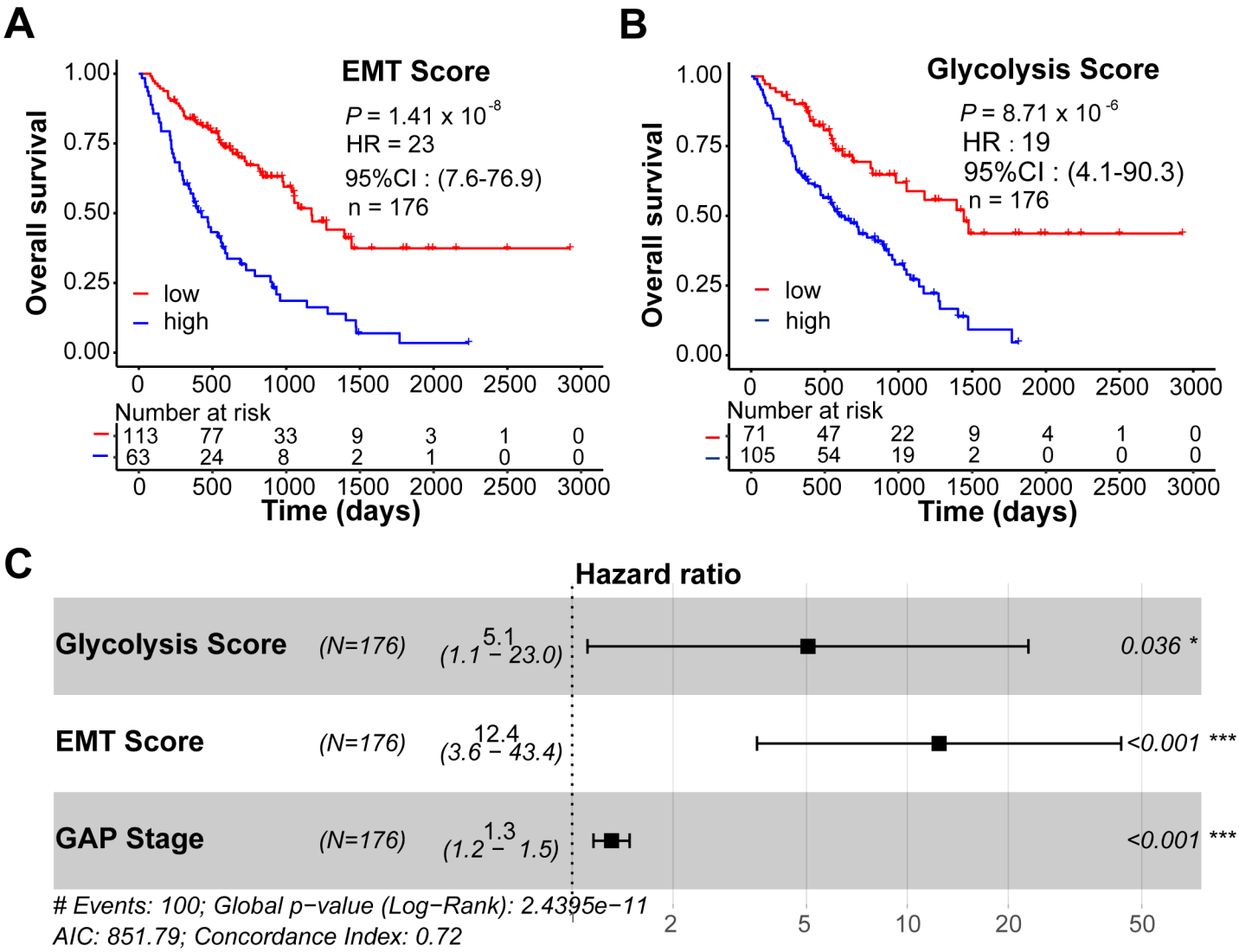
A
EMT Score
P = 1.41 x 10-8
HR = 23
95%CI : (7.6-76.9)
n = 176
Overall survival
low
high
Number at risk
113 77 33 9 3 1 0
63 24 8 2 1 0 0
Time (days)
B
Glycolysis Score
P = 8.71 x 10-6
HR : 19
95%CI : (4.1-90.3)
n = 176
Overall survival
low
high
Number at risk
71 47 22 9 4 1 0
105 54 19 2 0 0 0
Time (days)
C
Hazard ratio
Glycolysis Score (N=176) 5.1 (1.1 – 23.0) 0.036 *
EMT Score (N=176) 12.4 (3.6 – 43.4) <0.001 ***
GAP Stage (N=176) 1.3 (1.2 – 1.5) <0.001 ***
Events: 100; Global p−value (Log−Rank): 2.4395e−11
AIC: 851.79; Concordance Index: 0.72

Figure 3

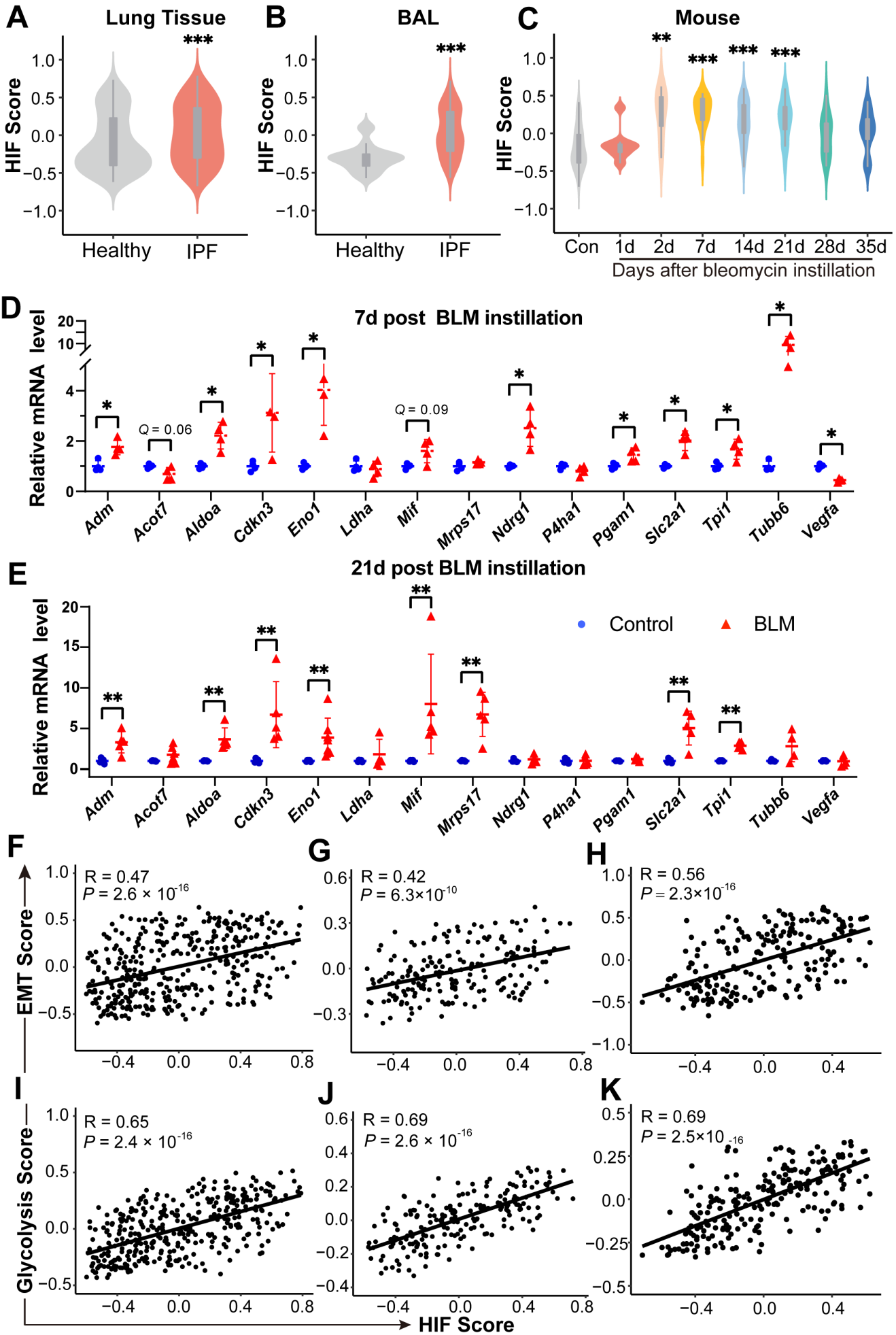
A
Lung Tissue
HIF Score
Healthy
IPF
***
B
BAL
HIF Score
Healthy
IPF
***
C
Mouse
HIF Score
Con
1d
2d
7d
14d
21d
28d
35d
Days after bleomycin instillation
D
7d post BLM instillation
Relative mRNA level
Q = 0.06
Q = 0.09
Adm
Acot7
Aldoa
Cdkn3
Eno1
Ldha
Mif
Mrps17
Ndrg1
P4ha1
Pgam1
Slc2a1
Tpi1
Tubb6
Vegfa
E
21d post BLM instillation
Relative mRNA level
Control
BLM
F
R = 0.47
P = 2.6 × 10-16
EMT Score
G
R = 0.42
P = 6.3×10-10
H
R = 0.56
P = 2.3×10-16
I
R = 0.65
P = 2.4 × 10-16
Glycolysis Score
J
R = 0.69
P = 2.6 × 10-16
K
R = 0.69
P = 2.5×10-16
HIF Score

Figure 4

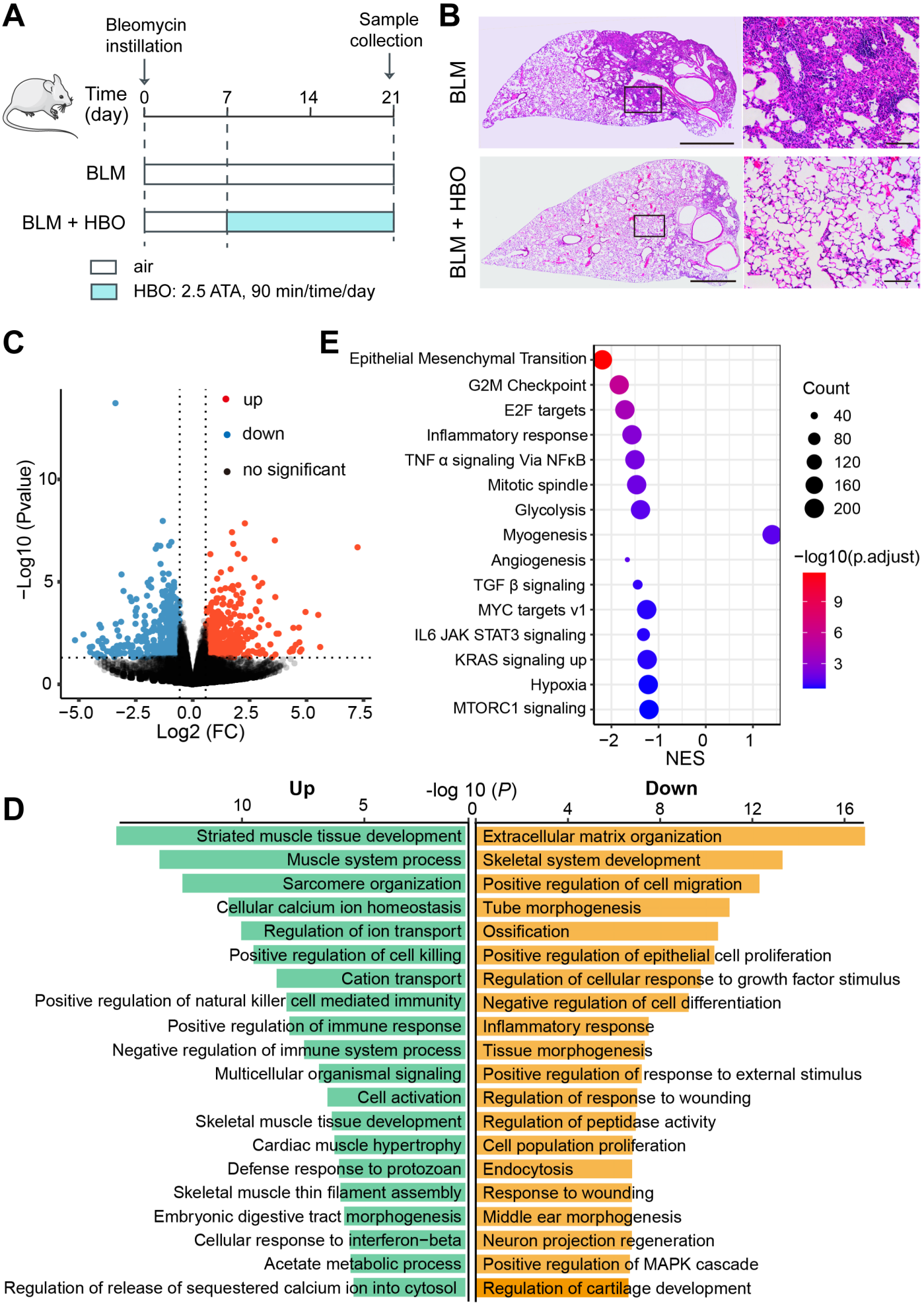
A
Bleomycin instillation
Sample collection
Time (day)
0
7
14
21
BLM
BLM + HBO
air
HBO: 2.5 ATA, 90 min/time/day
B
BLM
BLM + HBO
C
up
down
no significant
−Log10 (Pvalue)
Log2 (FC)
E
Epithelial Mesenchymal Transition
G2M Checkpoint
E2F targets
Inflammatory response
TNF α signaling Via NFκB
Mitotic spindle
Glycolysis
Myogenesis
Angiogenesis
TGF β signaling
MYC targets v1
IL6 JAK STAT3 signaling
KRAS signaling up
Hypoxia
MTORC1 signaling
NES
Count
−log10(p.adjust)
D
Up
-log 10 (P)
Down
Striated muscle tissue development
Muscle system process
Sarcomere organization
Cellular calcium ion homeostasis
Regulation of ion transport
Positive regulation of cell killing
Cation transport
Positive regulation of natural killer cell mediated immunity
Positive regulation of immune response
Negative regulation of immune system process
Multicellular organismal signaling
Cell activation
Skeletal muscle tissue development
Cardiac muscle hypertrophy
Defense response to protozoan
Skeletal muscle thin filament assembly
Embryonic digestive tract morphogenesis
Cellular response to interferon−beta
Acetate metabolic process
Regulation of release of sequestered calcium ion into cytosol
Extracellular matrix organization
Skeletal system development
Positive regulation of cell migration
Tube morphogenesis
Ossification
Positive regulation of epithelial cell proliferation
Regulation of cellular response to growth factor stimulus
Negative regulation of cell differentiation
Inflammatory response
Tissue morphogenesis
Positive regulation of response to external stimulus
Regulation of response to wounding
Regulation of peptidase activity
Cell population proliferation
Endocytosis
Response to wounding
Middle ear morphogenesis
Neuron projection regeneration
Positive regulation of MAPK cascade
Regulation of cartilage development

Figure 5

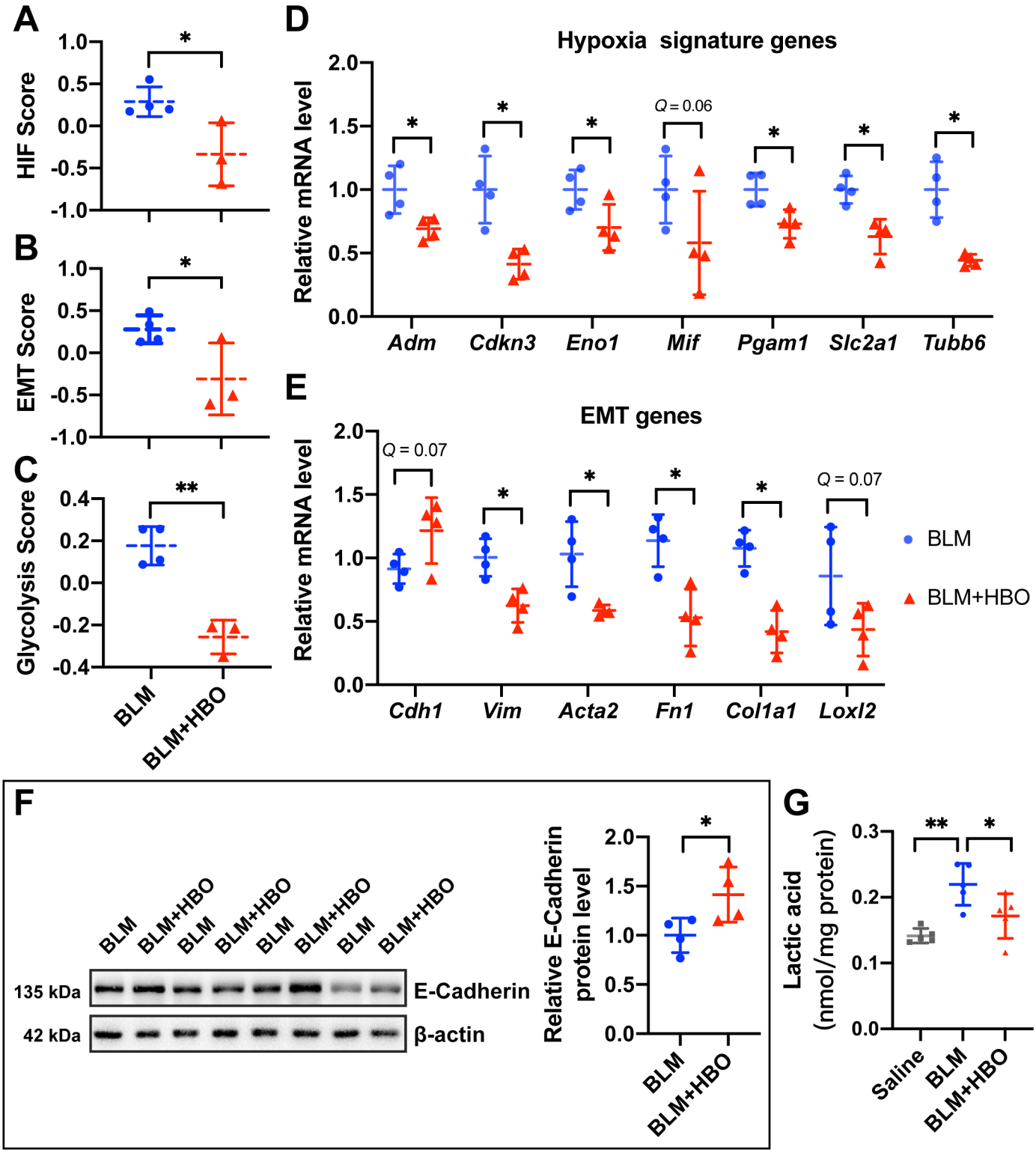
A
HIF Score
1.0
0.5
0.0
-0.5
-1.0
*
B
EMT Score
1.0
0.5
0.0
-0.5
-1.0
*
C
Glycolysis Score
0.4
0.2
0.0
-0.2
-0.4
**
BLM
BLM+HBO
D
Hypoxia signature genes
Relative mRNA level
2.0
1.5
1.0
0.5
0.0
*
Q = 0.06
Adm
Cdkn3
Eno1
Mif
Pgam1
Slc2a1
Tubb6
E
EMT genes
Relative mRNA level
Q = 0.07
Q = 0.07
Cdh1
Vim
Acta2
Fn1
Col1a1
Loxl2
BLM
BLM+HBO
F
BLM
BLM+HBO
135 kDa
E-Cadherin
42 kDa
β-actin
Relative E-Cadherin protein level
G
Lactic acid (nmol/mg protein)
0.3
0.2
0.1
0.0
**
*
Saline
BLM
BLM+HBO

Integrated analysis reveals the protective mechanism and therapeutic potential of hyperbaric oxygen against pulmonary fibrosis

Supplementary Materials

Table of contents

Supplementary Methods

1. Data collections

To collect the bleomycin-induced mouse model data, we searched the keywords "(mouse) AND (bleomycin) AND (pulmonary fibrosis)" and publication dates before 14/01/2022 in the National Center for Biotechnology Information (NCBI) Gene Expression Omnibus (GEO). Initially, 64 datasets were identified. Then we only included datasets that met the following criteria: 1) mRNA expression data; 2) lung tissue samples; 3) the pulmonary fibrosis mouse model was constructed via one dose intratracheal instillation bleomycin on a wildtype C57BL/6 background; 4) containing saline instillation control as well. Datasets generated on platforms other than Affymetrix, Agilent, or Illumina platforms were excluded to avoid the technical mismatch between different platforms. Datasets detected less than 10,000 genes were also excluded to balance the number of analyzed genes and sample size. GSE37635 is an exception, as it contains samples collected at 4 weeks and 5 weeks post bleomycin challenge that are barely detected in other datasets. Among these datasets, we only included samples from wildtype background and no more than 16-weeks old mice, and mice treated with control chemical combined with saline or bleomycin based on the clustering analysis. Three samples from the bleomycin group and one from the control group were excluded as they were mixed with the other group samples. Finally, a total of 10 datasets and 213 samples were included in the data merging analysis. The details of each dataset included are shown in Table S1, and the summary of data at different sample collecting timepoints is provided in Table S2.

To collect the IPF patients' data, we searched the keywords "(idiopathic pulmonary fibrosis) AND (Homo sapiens)" and publication dates before 14/01/2022 in the GEO database. Sixty-eight datasets were identified in the initial screening. Only the bulky mRNA sequencing data from human lung samples with a clear classification of healthy or IPF were included. Three datasets were excluded as the raw count datasheet was not available or format problem. Finally, a total of 6 datasets and 372 samples passed the inclusion criteria, and were described in Table S3.

2. Microarray data processing and differential expression gene (DEG) analysis

The raw gene expression data were imported into RStudio (version 4.1.0) and normalized based on microarray platforms. Affymetrix data were normalized via the RMA function[1] in affy (v1.66.0) packages, and Agilent microarrays were standardized by the function of normalizeBetweenArrays in limma (v3.44.3) package. Illumina beadchip array data were performed by the function of lumiExpresso in lumi (version 2.44.0). Microarray probe IDs were translated to gene symbols according to the GPL annotation files provided in the GEO database. Probes mapped to multiple gene symbols were removed and genes mapped to multiple probe IDs were summarized by calculating the mean. Expression data of the same conditions from multiple datasets were integrated. Only genes that are present across all the platforms remained for further analysis. Before further analysis, the batch effect was removed using the Combat function in the SVA package (version 3.4.0) following the default parameters.[2] Uniform manifold approximation and projection (UMAP) analysis was done through the umap package (version 0.2.7.0) and visualized by ggplot2 (version 3.3.5) package. Outliers were recognized as samples clustered in the wrong group by unsupervised hierarchical clustering (ward.D). Based on the results and the expected biological changes, three samples in the 21d bleomycin group and one sample in the control group were excluded from further analysis. DEGs were identified using limma package[3] (version 3.48.2) with the threshold adjusted $P < 0.05$ and fold change > 1.5. The volcano plots of DEGs were generated by the ggplot2 (version 3.3.5) package.

3. RNA-seq data merging and DEG analysis

The raw count data of lung tissues from IPF patients was downloaded from GEO datasets. The datasets were merged into one dataset using gene symbols as references. DESeq2 package was used to identify differential expression genes, the batch effect was estimated and subtracted in the algorithm. The threshold of DEGs was set as adjusted $P < 0.05$ and fold change > 1.5. RemoveBatchEffect function in limma (version 3.48.2) package was used to correct for the technical batch effect, and UMAP analysis was done through umap package (version 0.2.7.0) and plotted by ggplot2 (version 3.3.5) package.

4. Pathway enrichment analysis

Gene ontology (GO)[4] terms enrichment analysis of DEGs were generated through Metascape (https://metascape.org/gp/index.html#/main/step1) with default parameters. ClusterProiler (version 4.0.2) package[5] in the R software was used for gene set enrichment analysis (GSEA)[6] with the default parameters. The collection of hallmark gene sets generated from the msigdbr (version 7.4.1) package which covered the gene sets of Molecular Signature Database (MSigDB) was used for GSEA analysis. When the mouse data were analyzed, the gene symbols were translated to the human homologous genes first. *P* values adjusted by Benjamini-Hochberg (BH) method were used to estimate the statistical significance, $P_{adj} < 0.05$ and $P_{adj} < 0.25$ were defined as significant for GO enrichment and GSEA, respectively.

5. Pulmonary fibrosis model construction

SPF level male mice (C57BL/6) aged 6-8 weeks were used to construct the pulmonary fibrosis model. A single dose of bleomycin dissolved in 0.9% sterilized saline (2.0 U/kg, 40 μL, Hisun Pfizer Pharmaceutical Co., Ltd, Zhejiang, China) was instilled directly into the tracheal to induce pulmonary fibrosis in mice. Body weights were monitored every third day post bleomycin instillation. As reported in our previous study, mice with a weight loss of less than 5% on day 7 or less than 10% on day 10 post bleomycin challenge were considered as fail in the model construction, and were excluded from further study.[7]

6. HBO treatment

HBO exposure was applied as described previously.[8] Bleomycin-treated mice were randomized into control or HBO-treated group. HBO exposure (2.5 ATA, 90 min/day) was applied daily from day 7 after bleomycin instillation until day 20 in the HBO-treated group, while mice in the control group were untreated throughout the study. Lung tissue samples were collected on day 21 post bleomycin challenge.

7. Hematoxylin and eosin (H/E) staining

The left lung lobes of the mice were fixed with 4% paraformaldehyde for 24 hours, dehydrated by gradient ethanol, embedded in paraffin and sliced successively. Five μm thick slices were used for H/E staining, and a H/E stain kit (Beyotime Biotechnology, Shanghai, China) was used following the manufacturer's instructions. DM4000B microscope (Leica, Wetzlar, Germany) was used for imaging.

8. RNA-seq and bioinformatic analysis

The right lung lobes of the mice were used for RNA-seq. Total RNA was isolated using Trizol reagent (Invitrogen, Carlsbad, California, USA). A total amount of 3 μg RNA per sample was used for library construction. NEBNext® Ultra™ RNA Library Prep Kit for Illumina® (NEB, Ipswich, Massachusetts, USA) was used for sequencing libraries construction following the manufacturer's instruction. Libraries were sequenced using the paired-end strategy (2×150) on the Illumina NovaSeq 6000 platform following the standard protocols.

The quality control of the raw data was performed using FastQC (version 0.11.9) (https://www.bioinformatics.babraham.ac.uk/projects/fastqc) and MultiQC (version 1.8).[9] Trimming of the adapter content and reads with low quality (< 30) and short length (< 30 bp) was performed using Trim Galore (version 0.6.7) (https://github.com/FelixKrueger/TrimGalore). Hisat2 (version 2.2.0)[10] was used to map RNA sequence reads to the Ensembl GRcm38 *Mus musculus* genome, then samtools (version 1.9)[11] was used to transform sam files into bam files. FeatureCounts (version 2.0.0)[12] was used to summarize the read counts of each gene with default codes. Raw read counts were imported into RStudio and analyzed using the DESeq2 package. Genes with $P < 0.05$ and fold change > 1.5 were considered as DEGs.

9. Real-time qPCR analysis

Total RNA was isolated using TRIzol reagent (Invitrogen, California, USA), quantified with One Drop OD-1000+ Spectrophotometer (One Drop, Shanghai, China). HiScript II RT SuperMix for qPCR (+ gDNA wiper) (Vazyme, Jiangsu, China) was used for reverse transcriptions. Universal SYBR qPCR Master Mix was used for qPCR

detections (Vazyme, Jiangsu, China). Actb (β-actin) was used as the endogenous control to normalize the expression levels of target genes. Primers for the genes detected were as following:

Acot7-Forward: CGCTTTGTCCCATGTCTGCAA，

Acot7-Reverse: CATGGCAGCCCAGAATGTTT；

Adm-Forward: CACCCTGATGTTATTGGGTTCA，

Adm-Reverse: CCACTTATTCCACTTCTTTCGGA；

Aldoa-Forward: CTTAGTCCTTTCGCCTACCCACC，

Aldoa-Reverse: TTGAAGCTGGACCCATCTGGC；

Cdkn3-Forward: CCCTGATACATTGTTACGGAGGA，

Cdkn3-Reverse: CTCGAAGGCTGTCTATGGCTT；

Eno1-Forward: TATGCGCCTGCTCTGGTTA，

Eno1-Reverse: GTGCCGTCCATCTCGATCAT；

Ldha-Forward: AAGCACGTTGCTATGCCTTG，

Ldha-Reverse: GAACCCCAAAAGGGGATGGT；

Mif-Forward: TTGAGCCTCGCTCCACGTA，

Mif-Reverse: ATTTCTCCCGGCTGGAAGGTG；

Mrps17-Forward: GAGCGACCAGACTTGTTTTGG，

Mrps17-Reverse: GGCATCGTGAGCAAAGTAGG；

Ndrg1-Forward: TCAGGAGCAGGATATTGAGACC，

Ndrg1-Reverse: CCGATGTCGTGATACGTGAGG；

P4ha1-Forward: AGCCACCATTTCAAACCCAGT，

P4ha1-Reverse: GCCAAGCACTTTTGCTAATTCTG；

Pgam1-Forward: ATCTCGGCGATCCTCAGTTG，

Pgam1-Reverse: TGAAGCGGTTCTCCAGGTTC；

Slc2a1-Forward: GCAGTTCGGCTATAACACTGG，

Slc2a1-Reverse: GCGGTGGTTCCATGTTTGATTG；

Tpi1-Forward: CCAGGAAGTTCTTCGTTGGGG，

Tpi1-Reverse: CAAAGTCGATGTAAGCGGTGG；

Tubb6-Forward: TCCGAGTACCAGCAGTACCA，

Tubb6-Reverse: ACATGCTTAGACCAGGGCAC；

Vegfa-Forward: AACGATGAAGCCCTGGAGTG,

Vegfa-Reverse: GCTGGCTTTGGTGAGGTTTG;

Loxl2-Forward: CAGAGAAGACCTACAACCCCA，

Loxl2-Reverse: AGTGCCCGTGCAGTTCATAG；

Cdh1-Forward：CAGGTCTCCTCATGGCTTTGC,

Cdh1-Reverse: CTTCCGAAAAGAAGGCTGTCC;

Vim-Forward: TCAGCTCACCAACGACAAGG

Vim-Reverse: TTCAAGGTCAAGACGTGCCA

Mmp2-Forward: TCAGCTCACCAACGACAAGG

Mmp2-Reverse: TTCAAGGTCAAGACGTGCCA

Acta2-Forward: TCCCTGGAGAAGAGCTACGAAC,

Acta2-Reverse: AGGACGTTGTTAGCATAGAGATCC;

Col1a1-Forward: AGCACGTCTGGTTTGGAGAG,

Col1a1-Reverse: GACATTAGGCGCAGGAAGGT;

Fn1-Forward: CCCCAACTGGTTACCCTTCC,

Fn1-Reverse: TGTCCGCCTAAAGCCATGTT;

*β-acti*n-Forward: ACACCCGCCACCAGTTC，

β-actin-Reverse: TACAGCCCGGGGAGCAT.

Supplementary Figures

Figure S1. Flow charts showing the data collection process for lung samples from bleomycin-challenged mice **(A)** and IPF patients **(B)**. Details are provided in Supplementary Methods.

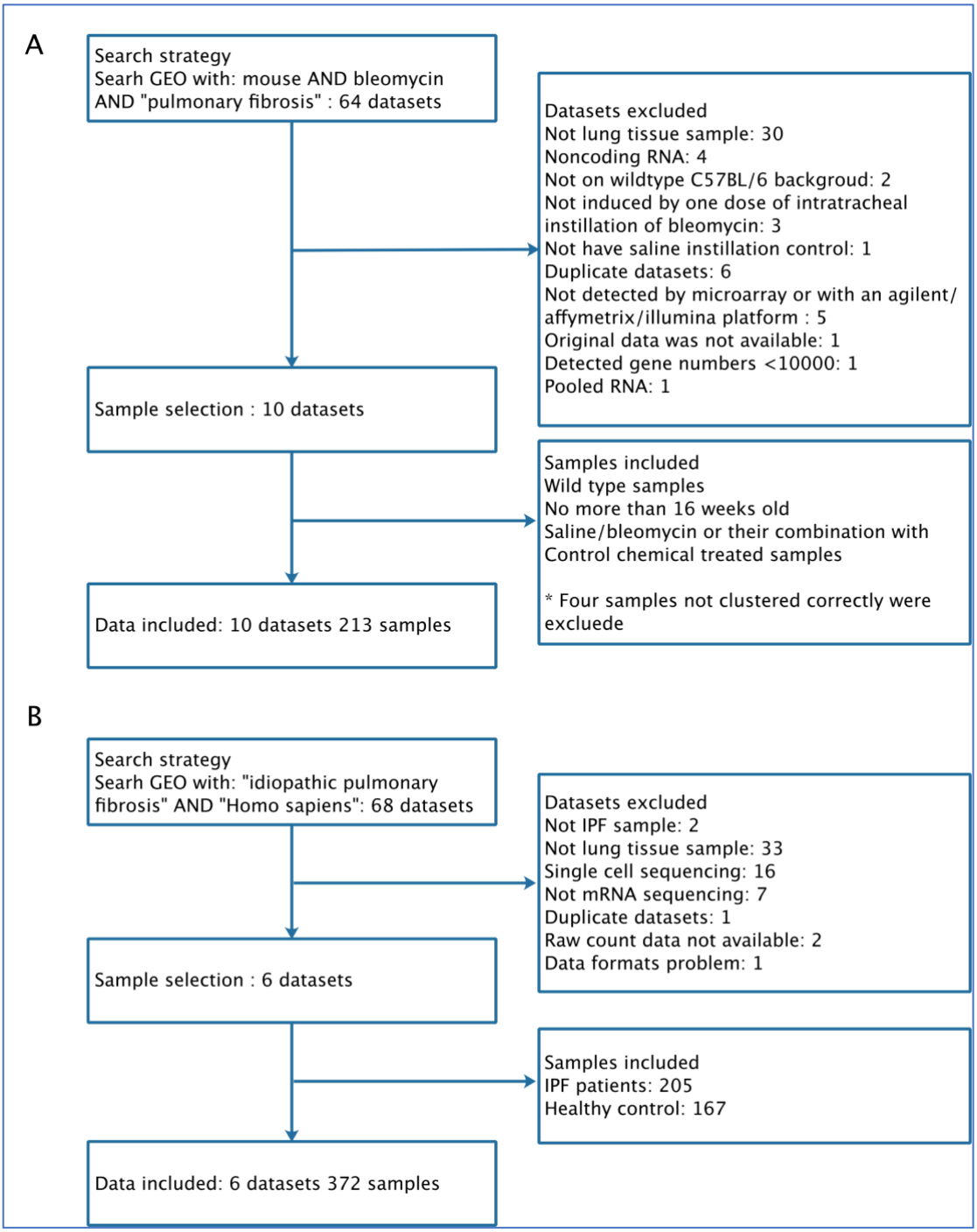

Figure S2. Batch effects removal by cross-platform normalization in microarray datasets from control and bleomycin-challenged mice lungs. UMAP plots showing samples from bleomycin-induced pulmonary fibrosis included in the integrative analysis before **(A, C and E)** and after **(B, D and E)** the removal of batch effects.

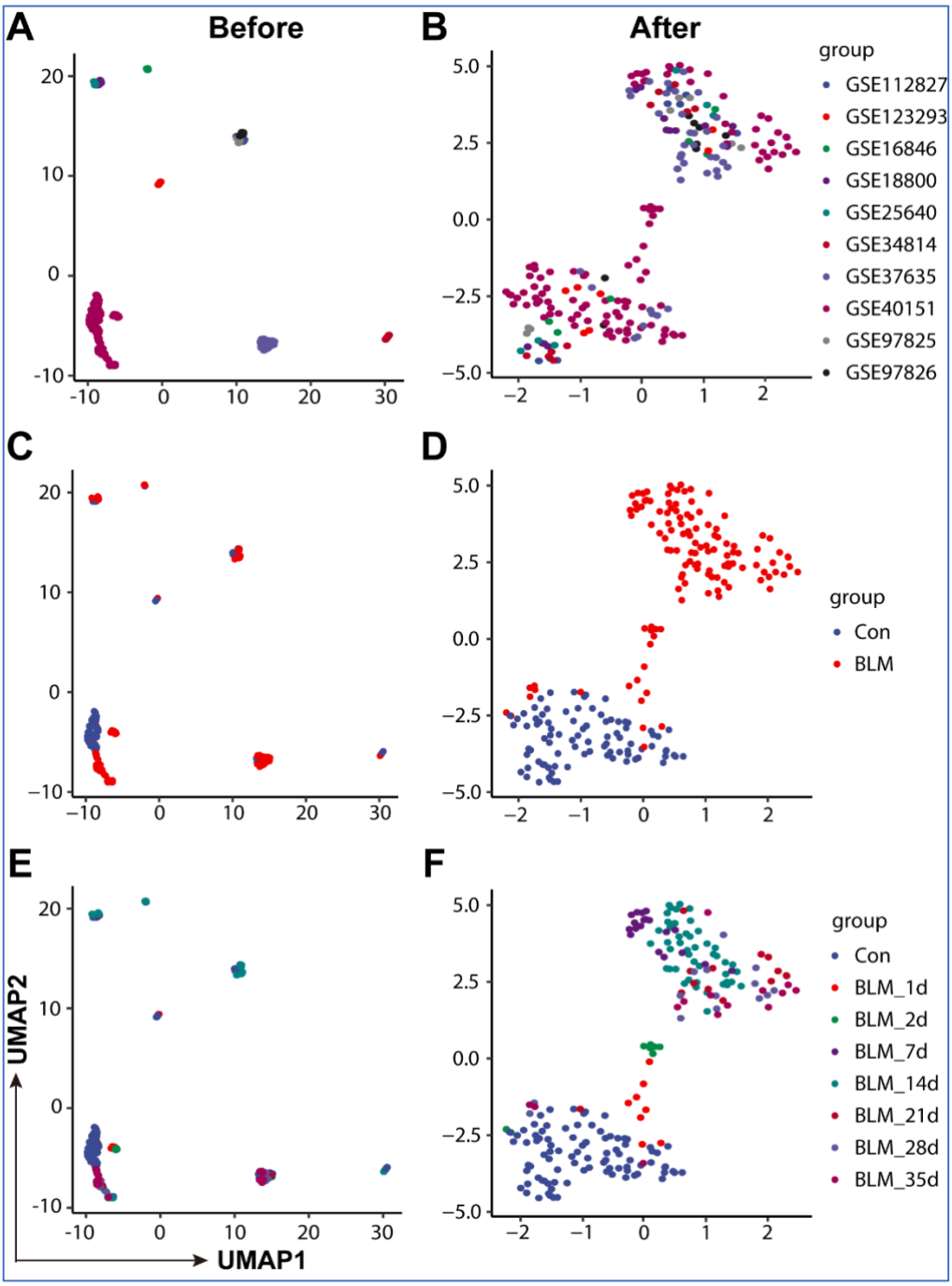

Figure S3. Batch effects removal in RNA-seq datasets from control and IPF lungs. UMAP plots showing samples from control and IPF lungs included in the integrative analysis before **(A and C)** and after **(B and D)** the removal of batch effect.

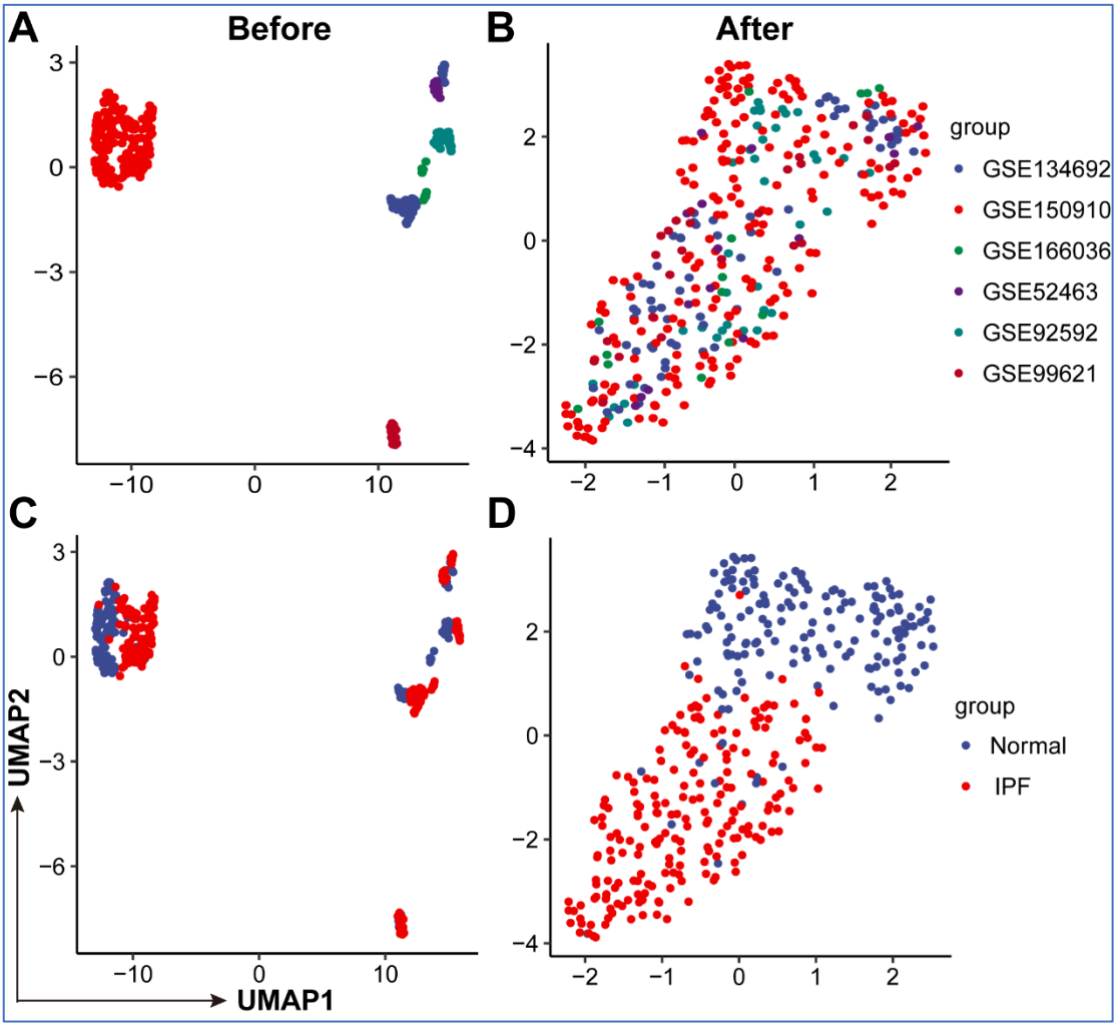

Figure S4. Integrative analysis identifies DEGs in pulmonary fibrosis. Volcano plots showing DEGs identified in bleomycin-challenged mice lungs at different time points post instillation **(A-G)** and in IPF lungs **(H)**. Up- and down-regulated (P_{adj} <0.05 and fold change > 1.5) DEGs are highlighted in red and blue, respectively.

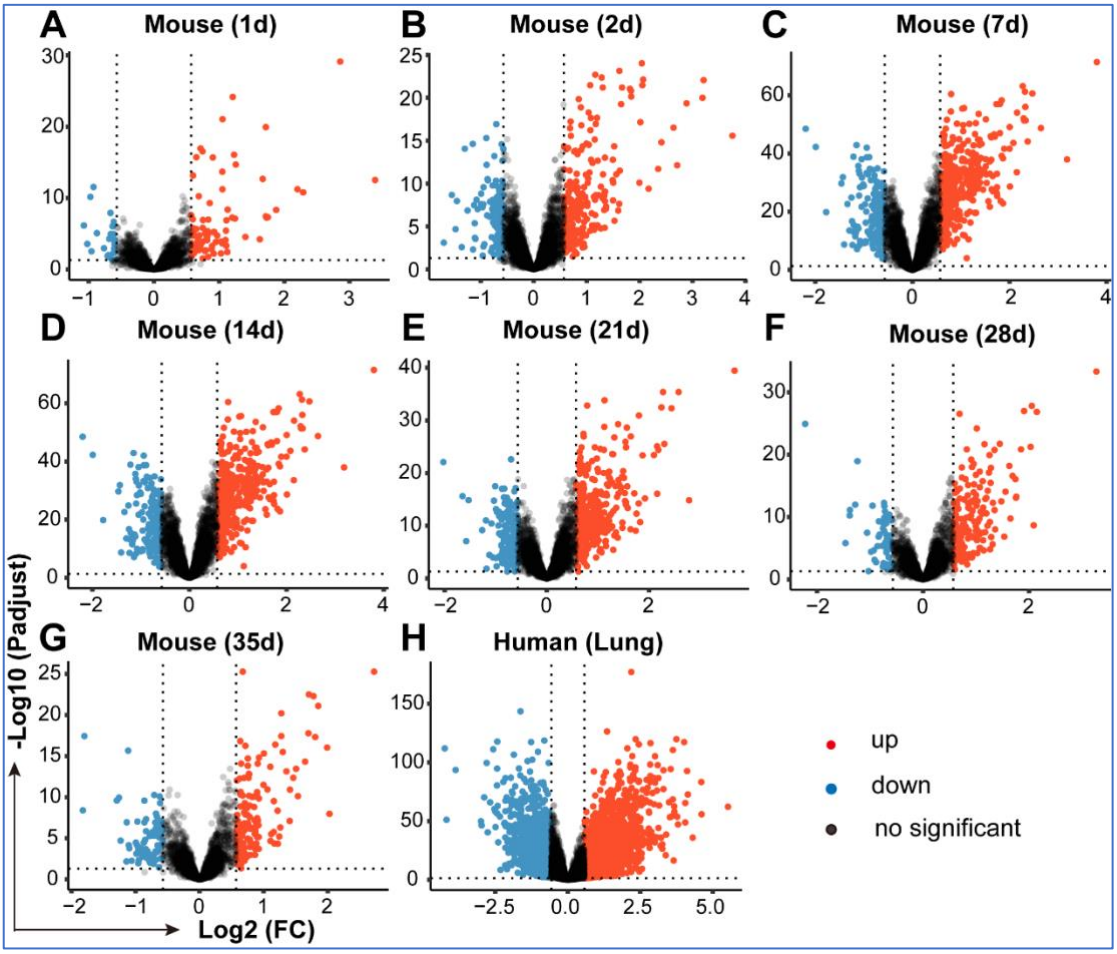

Figure S5. Bleomycin treatment induces pulmonary fibrosis in mice lungs. H/E staining of the lung tissue sections from saline (con, **A**) or bleomycin-challenged mice (BLM) at day 7 **(B)** or day 21 **(C)** post instillation. The top panel shows the whole left lung lobes section (scale bar: 500 μm) with higher magnification images in the bottom panel (scale bar: 100 μm).

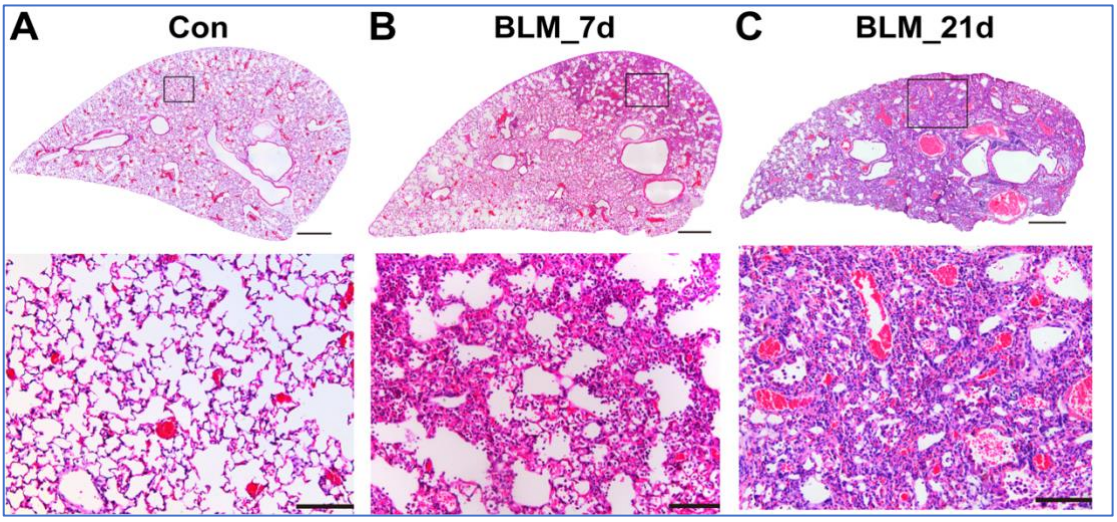

Supplementary Tables

Table S1. Datasets details of the bleomycin-induced fibrosis mice model.

Table S2. Time points information of the bleomycin-induced fibrosis mice model.

Table S3. Summary of the IPF datasets.

Table S4. DEGs in bleomycin-challenged mice lungs at day 1 post instillation.

Table S5. DEGs in bleomycin-challenged mice lungs at day 2 post instillation.

Table S6. DEGs in bleomycin-challenged mice lungs at day 7 post instillation.

Table S7. DEGs in bleomycin-challenged mice lungs at day 14 post instillation.

Table S8. DEGs in bleomycin-challenged mice lungs at day 21 post instillation.

Table S9. DEGs in bleomycin-challenged mice lungs at day 28 post instillation.

Table S10. DEGs in bleomycin-challenged mice lungs at day 35 post instillation.

Table S11. DEGs in IPF lungs.

Table S12. GO terms enriched in bleomycin-challenged mice lungs at day 1 post instillation.

Table S13. GO terms enriched in bleomycin-challenged mice lungs at day 2 post instillation.

Table S14. GO terms enriched in bleomycin-challenged mice lungs at day 7 post instillation.

Table S15. GO terms enriched in bleomycin-challenged mice lungs at day 14 post instillation.

Table S16. GO terms enriched in bleomycin-challenged mice lungs at day 21 post instillation.

Table S17. GO terms enriched in bleomycin-challenged mice lungs at day 28 post instillation.

Table S18. GO terms enriched in bleomycin-challenged mice lungs at day 35 post instillation.

Table S19. GO terms enriched in IPF lungs.

Table S20. DEGs in bleomycin-challenged mice lungs exposed to HBO.

Table S21. GO enriched in bleomycin-challenged mice lungs exposed to HBO.

References

1. Irizarry RA, Hobbs B, Collin F, et al. Exploration, normalization, and summaries of high density oligonucleotide array probe level data. *Biostatistics*. Apr 2003;4(2):249-64. doi:10.1093/biostatistics/4.2.249

2. Leek JT, Johnson WE, Parker HS, Jaffe AE, Storey JD. The sva package for removing batch effects and other unwanted variation in high-throughput experiments. *Bioinformatics*. Mar 15 2012;28(6):882-3. doi:10.1093/bioinformatics/bts034

3. Ritchie ME, Phipson B, Wu D, et al. limma powers differential expression analyses for RNA-sequencing and microarray studies. *Nucleic Acids Res*. Apr 20 2015;43(7):e47. doi:10.1093/nar/gkv007

4. Gene Ontology C. The Gene Ontology (GO) project in 2006. *Nucleic Acids Res*. Jan 1 2006;34(Database issue):D322-6. doi:10.1093/nar/gkj021

5. Yu G, Wang LG, Han Y, He QY. clusterProfiler: an R package for comparing biological themes among gene clusters. *Omics*. May 2012;16(5):284-7. doi:10.1089/omi.2011.0118

6. Subramanian A, Tamayo P, Mootha VK, et al. Gene set enrichment analysis: a knowledge-based approach for interpreting genome-wide expression profiles. *Proc Natl Acad Sci U S A*. Oct 25 2005;102(43):15545-50. doi:10.1073/pnas.0506580102

7. Yuan Y, Li Y, Qiao G, et al. Hyperbaric Oxygen Ameliorates Bleomycin-Induced Pulmonary Fibrosis in Mice. *Front Mol Biosci*. 2021;8:675437. doi:10.3389/fmolb.2021.675437

8. Yuan Y, Zhou Y, Li Y, et al. Deconvolution of RNA-Seq Analysis of Hyperbaric Oxygen-Treated Mice Lungs Reveals Mesenchymal Cell Subtype Changes. *Int J Mol Sci*. Feb 18 2020;21(4):1371. doi:10.3390/ijms21041371

9. Ewels P, Magnusson M, Lundin S, Käller M. MultiQC: summarize analysis results for multiple tools and samples in a single report. *Bioinformatics*. Oct 1 2016;32(19):3047-8. doi:10.1093/bioinformatics/btw354

10. Kim D, Langmead B, Salzberg SL. HISAT: a fast spliced aligner with low memory requirements. *Nat Methods*. Apr 2015;12(4):357-60. doi:10.1038/nmeth.3317

11. Li H, Handsaker B, Wysoker A, et al. The Sequence Alignment/Map format and SAMtools. *Bioinformatics*. Aug 15 2009;25(16):2078-9. doi:10.1093/bioinformatics/btp352

12. Liao Y, Smyth GK, Shi W. featureCounts: an efficient general purpose program for assigning sequence reads to genomic features. *Bioinformatics*. Apr 1 2014;30(7):923-30. doi:10.1093/bioinformatics/btt656